J. Indian Inst. Sci.
A Multidisciplinary Reviews Journal
ISSN: 0970-4140 Coden-JIISAD

REVIEW ARTICLE

Advances and Applications of Rapid Electrokinetic Patterning

*Mohamed Z. Rashed, Vanessa Velasco and Stuart J. Williams**

Abstract | The dynamic manipulation and assembly of colloids enables the advancement of analytical techniques in biotechnology and the development of self-assembled materials. Rapid electrokinetic patterning (REP) is a hybrid optoelectrokinetic technique that simultaneously uses a laser illumination and a uniform AC electric field to yield programmable, dynamic, and non-invasive manipulation of colloidal particles. Since it was introduced, the technique has been applied to microengineering and biological research fields, showing its promising capabilities as a great tool for trapping, aggregating, translating, and sorting single and multiple micro- and nanoparticles, including bacteria. To effectively leverage and enhance these applications, this review paper will highlight its versatility and capability, including REP's principles, governing physics, different experimental setups, fabrications, applications, and future prospects.

1 Introduction

The need to control micro and nanoparticles are essential in microfluidic platforms involving in vitro biological applications or general micro- and nanoparticle colloidal manipulation. Current manipulation techniques that offer a label-free control and manipulate such entities include active systems such as dielectrophoresis,[2, 27, 30, 37, 50, 54, 56] electrophoresis,[17, 31, 45, 82] optical trapping,[3, 11, 22, 86] acoustophoresis,[16, 40, 54, 64, 71] and hydrodynamic forces.[8, 19, 66, 69, 85] These techniques require an external stimulus that interacts with the intrinsic properties of the bio-particles including their dielectric properties, optical properties, morphology, and/or chemical state. Label-based techniques like magnetophoresis[1, 15, 55, 57, 62, 68] require extra labeling. Although these techniques revolutionized the biotechnology field with their capability of trapping,[13, 53] concentrating,[72] focusing,[9, 87] sorting,[7, 26, 56] separating,[4, 42, 84] detecting,[67] counting, lysing, and filtering[25] bio-particles, they either lack high resolution[5, 12, 41] or high throughput manipulation.[5, 65]

Bio-particles manipulated using aforementioned active label-free electrokinetic techniques require the application of a proper electric field to avoid unwanted electrokinetic effects. For example, a large electric field will harm the viability and growth of the cells being analyzed[43, 87] and is exacerbated when DC voltages or high voltages at lower frequencies are applied.[28] Another unfavorable factor that limits the application of higher electric fields is Joule heating which causes the local temperature of the medium to rise in response to the applied field. Joule heating is also responsible for the formation of bubbles inside the microchannels which compromise device performance. Jaeger et al. found that the electric field induced temperature rise is linearly proportional to increasing the electric conductivity of the medium. However, most of biological cells require suspension in high electric conductive media (>0.1 S m^{-1}). Hence, reducing buffer conductivity is required to suppress the Joule heating. High electric fields are required to enhance the range of dielectrophoretic force which decays far from planar electrodes. 3D electrode design can

[1] Department of Mechanical Engineering, University of Louisville, Louisville, KY 40292, USA. *stuart.williams@louisville.edu

Springer IISc Press

help to minimize dielectrophoretic force decay,[44] which will minimize the Joule heating 8–10 times lower than in planar electrode designs.[70] However, such design will add an additional fabrication cost and complexity. Hence, the current trend is to develop new electrokinetic techniques that use new fabrication methods or integrate additional physical mechanisms to synergistically achieve a wide range of resolution, high throughput, and robust non-invasive manipulation.

REP is a technique that merges the advantages of high resolution, dynamic manipulation of optical tweezers with the high throughput of AC electrokinetics resulting in precise, dynamic, and programmable control of colloids.[32, 79, 80] REP uses a parallel plate electrode system that provides AC electrokinetic forces and a highly focused laser beam that induces localized 'hot-spots' on the electrodes. Electrothermal flows are generated due to the sharp thermal gradients induced by the localized hot-spots. The application of the electric field acting upon these gradients, result in electrothermal hydrodynamic motion that carries the suspended particles towards the trapping region, achieving rapid accumulation and patterning at a desired location on the electrode surface. A variety of particles have been manipulated by Williams et al. using different schemes of optical landscapes (Fig. 1).[76] When both the laser irradiation and electric fields are applied, particles can be concentrated rapidly within the irradiated spot (Fig. 1b), the size of cluster can be modulated by either increasing the size of the irradiated spot or the intensity of laser illumination. Not only can REP trap and concentrate micro- and nanoparticles but it can also translate and concentrate them at any desired spot on the electrode (Fig. 1c, g, i).

REP colloidal accumulation is frequency dependent, enabling selective concentration of particles as well as sorting (Fig. 1f).[78] In the low frequency regime (< 200 kHz) Williams et al. successfully trapped and dynamically patterned micrometer particles on an indium tin oxide (ITO) electrode surface by utilizing various optical schemes produced from a laser operating at a wavelength of 1064 nm. REP is a versatile technique and particles as diverse as silica particles[81] and polystyrene particles[80] (50 nm–3 μm) have been successfully assembled. REP offers significant benefits to lab-on-a-chip (LOC) systems devised for biological or chemical analysis. Conducting high accurate analysis and throughput by implementing REP will improve the performance of biochemical sensors, diagnostic biochemical devices for biological assays,[38, 76] enhanced detection for diabetic retinopathy,[75] as well as trapping and deposition of multiwalled carbon nanotubes.[47]

REP is a novel technique with high potential and capabilities to be integrated to enhance various biological, biotechnological and lab-on-a-chip fields. This review article will: (1) highlight the efforts done by researchers to provide physical understanding of REP through experimentation and modelling as well as characterizing its electrokinetic mechanisms, (2) summarize the initial experiments and results of REP showcasing its potential, and attempted applications, and (3) discuss current challenges, future opportunities, and alternative inexpensive REP platforms.

2 REP Setup and Operation

In a REP chip, two conductive ITO-coated transparent glass plates are separated by a suitable spacer (50–100 μm) such as a commercial double side adhesive tape patterned with a razor or laser cutter. Inlet and outlet reservoirs were achieved by drilling through the (Fig. 2a)[33, 76, 79, 80] ITO-coated transparent glass substrates which were used in parallel with different metal-coated glass plates, in both cases the laser irradiated spot was applied on either plate. However, as ITO has a high electrical resistance, other more conductive metals such as copper, gold, and a chrome-coated electrode also may be used (Table 1). The chosen conductor needs to absorb sufficient illumination to induce electrothermal flow, applications of REP have primarily used ITO with NIR (1064 nm) illumination (Fig. 2b)[33, 35, 75–77, 79, 80] the media itself does not directly absorb significant laser illumination.

The optically induced temperature gradient generates gradients of conductivity and permittivity that coupled with the applied AC electric field creates a toroidal electrothermal vortex (Fig. 2a). A crucial parameter to consider in the experimental setup is optical skin depth of the electrode material being used; each material has an optimal thickness that can achieve highest absorption of the laser irradiation, for ITO material this thickness is approximately 700 nm with an absorption coefficient of 1.3×10^5 m^{-1},[29] which is greater than the typical ITO thickness commercially available (350 nm). Nickel, with its higher absorption coefficient than ITO (5.59×10^7 m^{-1}) and optical skin depth of 17.9 nm, has been tested and showed 2.4×10^4 K W^{-1} (Kelvin per laser power) while titanium was found to be 3.5×10^4 K W^{-1} with an optical skin depth of 21.06 nm.[29, 48] At the same laser power, titanium will absorb laser

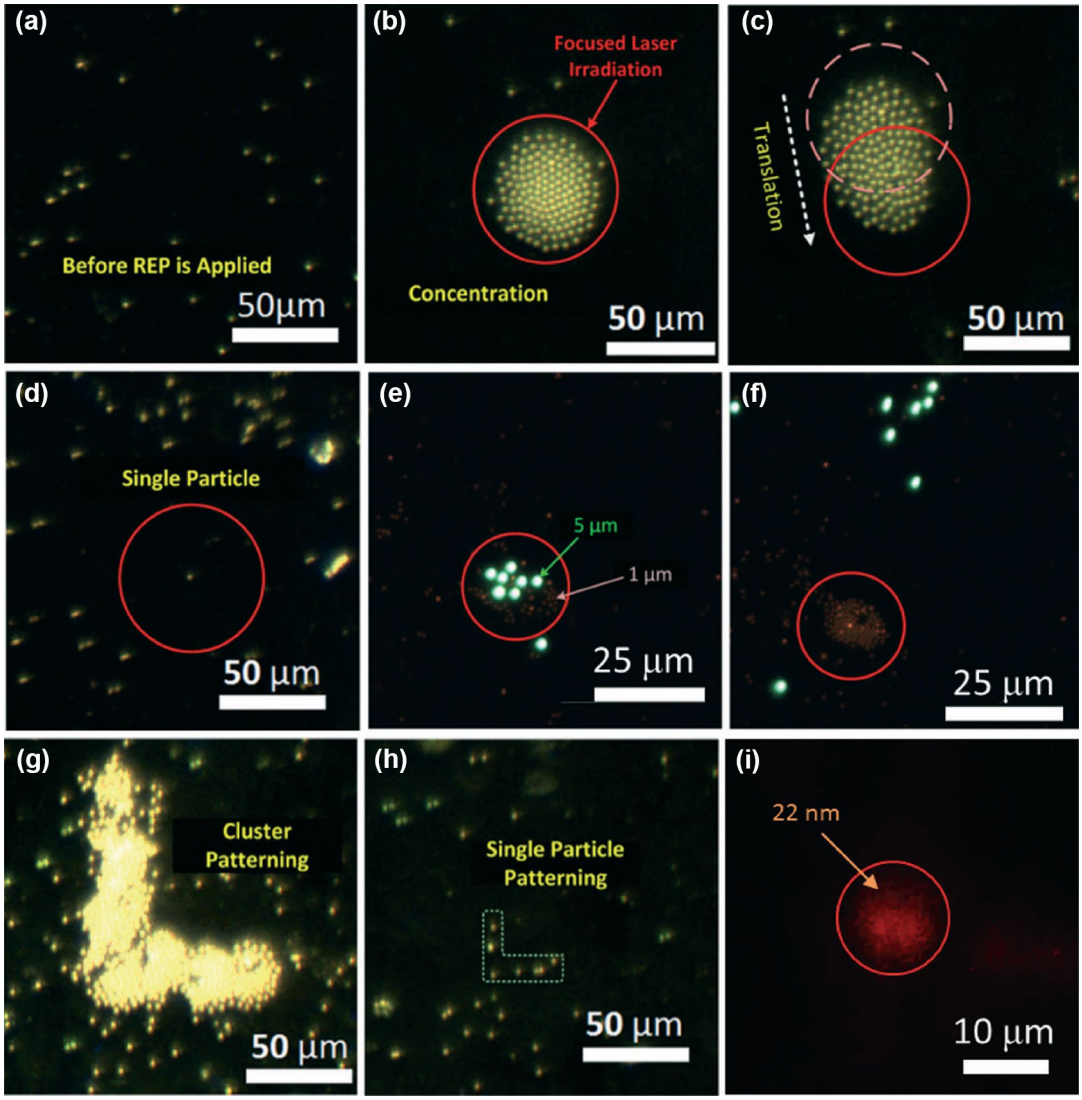

Figure 1: Particles manipulated with REP: **a** no trapping of particles in the initial state, **b** aggregation of 5 μm particles at 5 kHz, **c** translation of 5 μm trapped particles at 5 kHz, **d** single particle manipulation (5 μm) at 17 kHz, **e** simultaneous trapping of 1 and 5 μm particles at 5 kHz, **f** 1 μm particles sorted by size at 36 kHz, **g** L-shaped patterning of 5 μm particles, **h** single particle patterning (5 μm particles), and **i** 22 nm particle aggregation at 5 kHz and 16.5 V_{pp}. Reproduced with permission of the Royal Society of Chemistry[76].

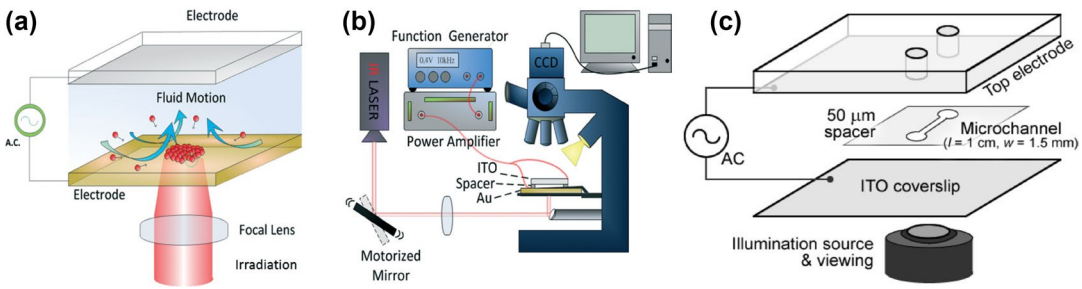

Figure 2: **a** Illustration of REP operation. **b** Schematic of the experimental setup. **c** Microchannel formation sandwiched between the parallel ITO electrodes. **a**, **b** Reproduced with permission of the Royal Society of Chemistry.[76] **c** [78].

Table 1: Reported REP experimental conditions.

AC frequency	1–200 kHz		
Applied electric field	6×10^4–5×10^5 V_{pp} m^{-1}		
Diameter of manipulated particles	0.05–3 μm		
Buffer conductivity	< 150 mS m^{-1}		
Heating method	Laser illumination $\lambda = 532$ nm	Gold-coated electrodes (6.4–150 nm thick)	
	Laser illumination $\lambda = 1064$ nm	ITO coated electrodes (0.7 μm thick)	20–30 mW
			Max temperature increase < 10 °C
	Resistive heating	Copper/gold	Max temperature increase 18 °C and gradient 0.5 °C μm^{-1} with 1.6 V_{pp}

irradiation higher than nickel or ITO, hence it will generate higher thermal gradients which will generate greater electrothermal flow. Therefore, an expensive high-power laser source may be replaced with inexpensive optical source to generate the illumination required to induce the thermal gradient.[29, 48, 78] This feature is crucial as it allows REP to conduct at different optical wavelengths, provided that a proper combination of laser power, wavelength, and electrode material is chosen to generate the necessary optically induced temperature gradients.[35, 48, 78]

The programmable laser source in REP dynamic operation is typically applied using a hologram generated from a spatial light modulator or scanning laser system,[74] being focused by a high numerical aperture objective lens. Low conductivity buffers were used, typically deionized water[33, 34, 38, 78–80] conductivities up to 150 mS m^{-1} has been attempted though are not seemingly viable as some of the governing electrokinetic mechanisms are suppressed at elevated conductivities (see next section). Further, in the case of using a high conductivity electrolyte ($\sigma > 200$ mS m^{-1}), Joule heating will need to be monitored. However, it is important that future REP platforms be applied towards moderate (~ 100 mS m^{-1}) or high conductivity media to handle an assortment of biological cells.

3 Physical Mechanisms of REP

As REP operation is a hybrid opto-electrokinetic mechanism, it requires a simultaneous application of a uniform AC electric field as well as laser illumination. REP particle trapping is achieved by a precise balance of several electrokinetic forces. First, bulk electrothermal flow is generated at the center of the illumination. The laser induces nonuniform thermal gradients in the medium causing local changes in fluid conductivity and permittivity which respond to the applied field. Natural convective flow is generally negligible for this microfluidic system.[24, 30, 31, 39, 81] Second, particle-induced AC electroosmosis (ACEO) is an electrohydrodynamic (EHD) mechanism that influences particle–electrode and particle–particle interactions.[34, 78, 81] Thanks to the synergetic effect between these two mechanisms trapping and patterning is possible using REP.

The time-averaged expression for this electrothermal body force is[20]

$$\langle F_e \rangle = {}^1/_2 \mathrm{Re}\left(\frac{\sigma \varepsilon (\alpha - \beta)}{\sigma + i\omega\varepsilon} (\nabla T \cdot E) E^* - {}^1/_2 \varepsilon \sigma |E|^2 \nabla T \right), \quad (1)$$

where Re() refers the real part of the expression, E is the electric field, E^* is its complex conjugate, T is the temperature, ω is the applied frequency, σ is the conductivity of the fluid, ε is the permittivity of the fluid, β is $(1/\sigma)(\delta\sigma/\delta T)$ and α is $(1/\varepsilon)(\delta\varepsilon/\delta T)$. The first and second term in (1) is the Coulomb force and the dielectric force, respectively; the first term will dominate until the frequency exceeds the charge relaxation of the fluid. Each term is dependent on the magnitude of the temperature gradients (∇T) which can be generated through Joule heating[20] or illumination.[21, 36, 49] The latter drives fluid motion within REP and, further, bulk Joule heating is neglected since the fluid conductivity is low and the applied field is uniform; therefore, the electrothermal body force scales as the second power of the electric field ($|E|^2$).[60, 78] One special case of REP

heating has the source of non-uniform heat from micro-patterned DC heaters.[73]

There exist a variety of frequency-dependent electrokinetic and electrohydrodynamic interactions in REP. These forces are grouped into four types (Fig. 3a)[76]: (1) particle–electrode attraction force, F_e, (2) dipole–dipole repulsion force, F_r, (3) drag force induced from the electrothermal flow (lateral, F_a and vertical, F_d), and (4) particle–particle EHD attraction, F_a.[52, 61] All of these electrokinetic forces are a function of AC frequency; therefore, a proper frequency needs to be chosen to balance these forces.[81] This is because at lower frequencies F_d is constant and it helps to drag the particles near the electrodes surface. Next, F_e results in trapping particles on the electrode surface where their crystallinity, aggregation and spacing is governed by F_a. As frequency increases, F_a weakens and the dipole–dipole resistive force, (F_r) increases interparticle spacing until the frequency reaches the particle's critical frequency at which time it is released from the electrode surface. Aggregation characteristics are a function of the particle size, particle surface charge, and the applied field amplitude and frequency. At high frequencies (>1 kHz) a low-density phase was observed while at low frequencies compact disconnected particle aggregations occurred. At higher frequencies particles are swept away from the accumulated cluster by the electrothermal flow force due to the relaxation of particle–electrode forces. There is a critical frequency for maintaining REP aggregations and is related to the polarization of the particles' electrical double layer.[33, 52, 78] Therefore, REP can be used to trap and sort particles based on their frequency-dependent double-layer polarization behavior. Once the applied frequency approaches the critical frequency the particle cluster becomes unstable and is swept away by electrothermal flow. A particle's critical frequency decreases with increasing particle size (Fig. 3b), specifically the particle–electrode force has an inverse dependence on the surface area of the particle. This critical frequency is key factor for separating or sorting colloidal particles applications.

Williams et al.[81] demonstrated the separation of 1 μm from 2 μm spheres by retaining the smaller particles at lower frequencies. Kwon et al.[38] performed separation of *Staphylococcus aureus* (*S. aureus*) bacterium (~1 μm in diameter) from *Saccharomyces cerevisiae* (*S. cerevisiae*) (~5 μm in diameter) based on their sizes.

Table 2 summarizes the main REP electrokinetic mechanisms with their underlying physics including their dependence on frequency. The electrohydrodynamic mechanism leading to compact particle aggregations is derived from field perturbations caused by the interaction between the polarized particle and electrode. The induced imbalance of charge on the electrode polarization layer causes local EHD. Ristenpart et al.[61] predicted that these electrohydrodynamic forces scaled with the square of the electric field strength (E^2) and the inverse of frequency (ω^{-1}). The dipole–dipole repulsive force is an additional particle–particle interaction that scales with the square of the electric field (E^2) and to the sixth power of the particle radius (a^6). This relationship provides a good estimation of particle forces for applied AC frequencies greater than 500 Hz.[14] Within REP, the dipole–dipole repulsive force becomes dominant at higher frequencies as particle–electrode EHD are suppressed.

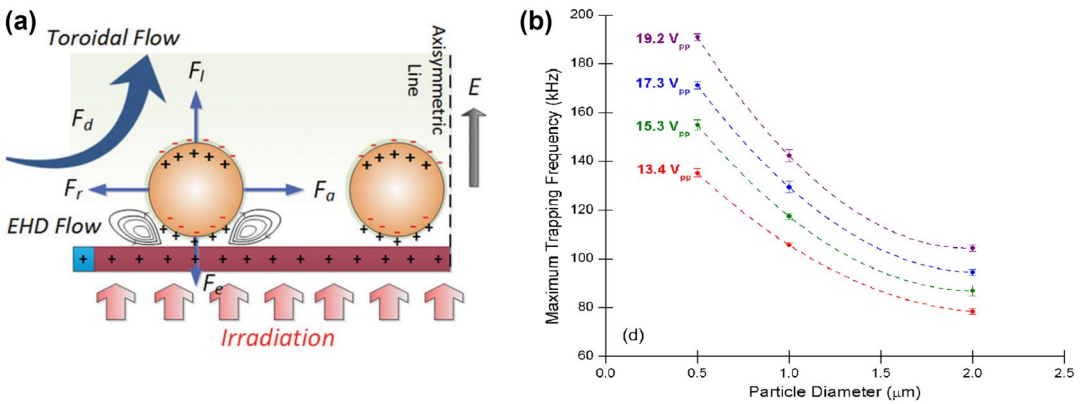

Figure 3: **a** Various electrokinetic forces involved in REP technique. **b** The critical frequency dependence on applied voltage and particle diameter. **a** Reproduced with the permission of Royal Society of Chemistry.[76] **b** Reproduced with the permission of American Institute of Physics[81].

Table 2: REP mechanisms with their underlying physics, scaling, and range of frequency dependence.

Mechanism	Observed behavior	Physics	Scaling	Citation
Electrothermal fluid motion (F_D)	Inward fluid vortices generated at the center of the focused laser Transports particles near the electrode surface Lateral drag to compact trapped particles	Local change in permittivity and conductivity induced by laser Gradients in dielectric properties combined with the electric field induce fluid motion First term in (1) is dependent on frequency, the second term is negligible in REP	Effectively, fluid motion is constant at low frequencies with; $F_D \propto$ heating power ($\sim \nabla T$) $F_D \propto E^2$ F_D is independent on particle size or type Until the fluid's charge relaxation is met ($\omega > 5$ MHz), then decreases and become negligible	6, 78
Particle–electrode electrokinetics (F_E)	Takes place at low frequencies and results trapping particles on the electrode surface	Particle-induced field gradients near the electrode surface induce localized EHD	Critical frequency above which particles cannot be held in the REP trap $\omega_c \propto 1/$particle surface area (a^2) $F_E \propto E^2$ $F_D \propto 1/$(distance from electrode)	14, 60, 81
Particle–particle electrokinetics	Frequency governs crystallinity of the aggregation	Controlled by attractive particle-induced EHD (F_a) and repulsive dipole–dipole forces (F_r).	F_a, $F_r \propto E^2$ At low frequencies: F_a is governed by local EHD flow and particles aggregate At high frequencies: EHD is suppressed and F_r is dominant; $F_r \propto a^6$ $F_r \propto 1/\sigma$	60, 78

Williams[78] studied REP particle–particle interactions and investigated its influence on inter-particle distance within aggregations.[83] They also established that there exists a frequency where a minimum distance is observed for different particles size. They also observed that the particles on the perimeter of the aggregation were spaced further apart from their neighbors due to the weaker hydrodynamic drag they experienced further from the vortex's center. They also revealed that particle–particle distance was independent of voltage since the aforementioned electrokinetic mechanisms (ACEO, electrothermal hydrodynamics, dipole–dipole repulsive forces) scale with the square of the applied electric field.

By altering the AC frequency, a myriad of particle–particle electrokinetic interactions can be achieved, particularly for solutions with different particle sizes. When the particle–particle distance reaches its minimum value, compact structures resulted in a semi-stable aggregate that held firmly to the electrode surface, resisting further hydrodynamic drag from the microfluidic vortex. Smaller particle aggregations tend to form multiple layers[80] whereas particles greater than 1.0 μm in diameter remain arranged as a monolayer aggregation.[78] The role of particle diameter and surface chemistry need to be investigated further to enable the creation of precisely tuned artificial architectures such as reconfigurable colloidal crystals. For example, since dipole–dipole forces scale with a^6, even larger particles (~ 10 μm) can form chains in the direction of the field (aka "pearl chaining"[10, 58, 59] while their assembly can be guided by bulk electrothermal flow, resulting in the generation of 3D assembled structures.

Work and Williams[83] investigated the particle-to-particle spacing for an REP aggregation as a function of laser-scanning length. They found that the average particle–particle spacing has a linear relationship with the length of the scanning laser. As long as the heating induced optically is evenly distributed across the scanned line, that linear relationship should be valid, maintaining a steady microfluidic vortex profile. Thus, upon decreasing the induced temperature gradients, particles become more spaced apart at increasing scan lengths due to the resultant decreased hydrodynamic drag. Additional information on REP mechanisms, including the critical frequency, patterning and crystallinity are available in previous publications.[33–36, 74, 78, 79, 80, 83]

4 REP Applications

The promising abilities of REP have been shown in different applications including the aggregation, translation, sorting, and patterning of single and multiple artificial micro and nanoparticles, as well as, viable particles such as bacteria. The following will provide an overview (Table S1) of the published material on the use of REP in these diverse applications.

4.1 General Patterning/Shape Modulation

For most initial REP demonstrations, the optical light source consisted of a focused light beam, where particles were arranged within a circular spot (Fig. 1b). However, patterning particles into more complex geometries is also possible[73, 79] and applicable in investigations of artificial structures involving colloidal crystalline assemblies. One REP example utilizes the conventional parallel plate ITO chip (Fig. S1), and an illumination source consisting of a near infrared holographic system. The shapes of the holographic optical landscapes were controlled by computer-programmed spatial light modulators that modified and replicated different light patterns. As a demonstration, Williams et al. showed a polystyrene (690 nm) particle assembly in the shape of an "L" (Fig. 4a, b).[79] In these experiments, REP was carried out with an AC signal of 2.0 V_{pp} at 1.6 kHz and an illumination intensity of 20 mW. By increasing the illumination intensity and voltage, larger trapping regions and particle aggregations were generated. Though the example only portrays polystyrene particles, similar observations were seen for latex and silica particles ranging from 300 nm to 3 μm.

Complex geometries of particle aggregations have also been achieved using a modified REP chip, containing thin film heaters (Fig. 4c–f).[73] The benefits of the thin film REP devices include its cost-effective thermal efficiency, simple/scalable fabrication, potential for higher throughput, and ability to integrate with other microsystems. In this modified REP chip, arrays of micropatterned thin films of copper were embedded within a glass substrate. The copper thin films are used as DC controlled heaters to create highly non-uniform temperature fields. Particles were assembled in the shape of the heater geometry, either a line (Fig. 4c, d) or "X" (Fig. 4e, f) wire trace at 10 V_{pp} and 100 kHz with 1.6 V_{DC} applied to the heaters. The thin film heaters make it possible to have several simultaneous trapping areas within a single platform. Initially, a single layer of particles (1 μm) were assembled. As the number

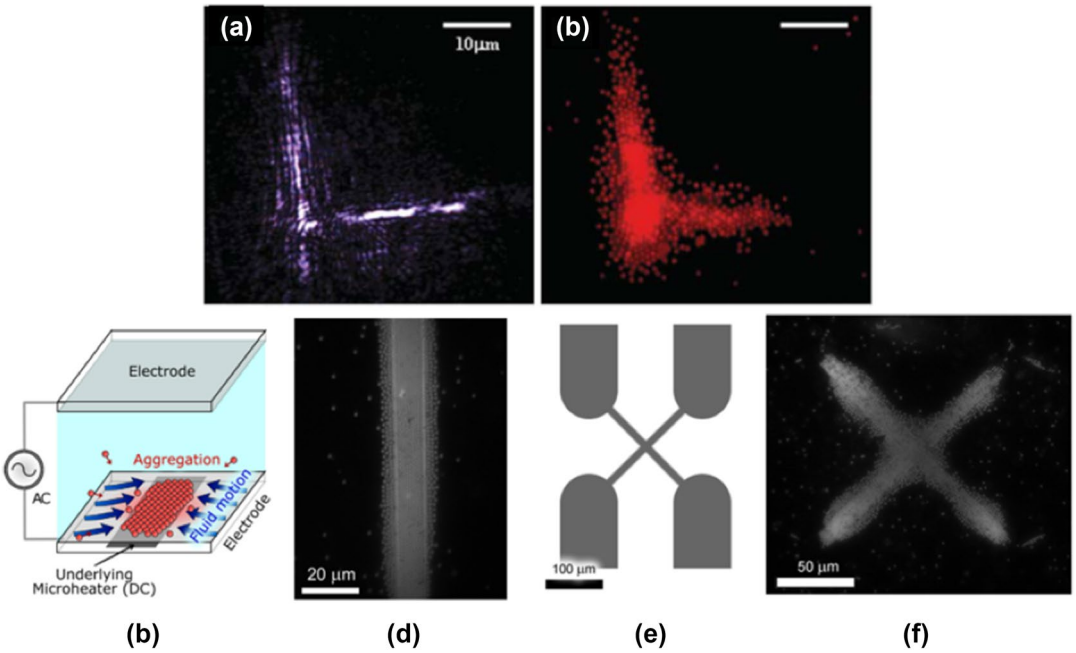

Figure 4: Depictions of complex geometries formed with REP: **a** optical landscape and **b** respective polystyrene particle (690 nm) assembly in the shape of an "L" with an AC signal of 2.0 V_{pp} at 1.6 kHz and an illumination intensity of 20 mW. Reproduced with permission of the Royal Society of Chemistry.[79] **c** Schematic of REP thin film heater device during particle aggregation. Particles were shown to assemble in the shape of the heater geometry. **d** For the line heaters, 1.0 μm particles were trapped at 1.6 V_{DC}, 10 V_{pp}, and 100 kHz. **e**, **f** Devices with "X" heaters accumulated particles at 1.6 V_{DC}, 10 V_{pp}, and 110 kHz. Reproduced with permission of Elsevier[73].

of particles trapped increased, a second and third layer of particles were collected, forming triangular tetrahedrons due to decreased drag and attractive dipole–dipole interactions.

REP can also be used to trap a particle cluster near the electrode surface in the simultaneous presence of bulk fluid flow.[79] Using the holographic optical illumination system and parallel electrode ITO platform, latex particles (1 μm) were assembled on the electrode surface at an AC signal of 10 V_{pp} at 5 kHz, illumination intensity of 40 mW, and pressure driven bulk fluid flow at 120 μm s^{-1}. The combination of REP and bulk microchannel flow will result in a concentrated stream of microparticles along the electrode surface. This ability has potential benefits in improving the performance of sensor-based lab-on chip systems, where the sensors are located along the surface of the microchannel.

Despite the dynamic benefit of REP that allows for particle clusters to be reconfigured into various shapes and translated to new areas in the electrode surface, these aggregations will disperse with the deactivation of the applied illumination pattern or AC field. However, particle assemblies can be permanently adhered to the electrode surface through the brief application of a DC offset voltage of 2.5 V.[23, 47, 79] It has been postulated that this phenomena results from electrophoretic forces manipulating the particles close to the substrate such that van der Waals forces permanently immobilize particles onto the substrate.[18] This ability to permanently pattern particles onto the electrode surface enables REP to be useful in area of colloidal assembly for micro and nano-manufacturing.

4.1.1 Patterning Nanoparticles

REP also has the ability to aggregate nanoparticles (Figs. 1i, 5). Unlike optical trapping techniques which are limited by Brownian motion and weak optical trapping forces, REP has been shown to concentrate and assemble polystyrene particles with diameters of 49–100 nm[78] as well as gold and silver nanoparticles with diameters of 40–200 nm.[47] The details on the constitution of the REP chip and experimental setup can be found in Williams.[78] For nanoparticle aggregation, an illumination intensity of 0.18 W and an AC signal of 14 V_{pp} at 10 kHz trapped 100 nm particles in a single spot on the gold electrode

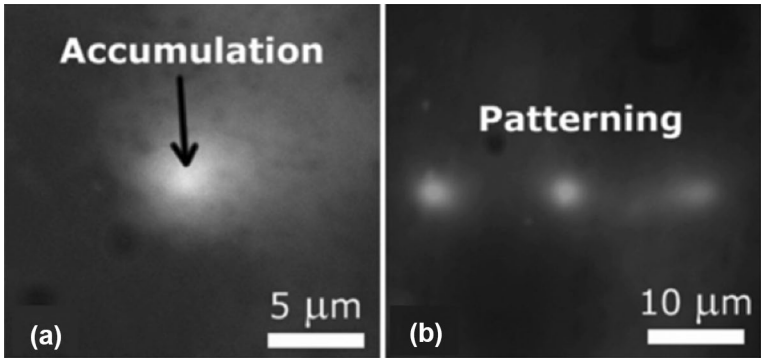

Figure 5: Illustrations of 100 nm nanoparticles captured within a **a** single laser spot at 0.18 W and an AC signal of 14 V_{pp} at 10 kHz and **b** three laser spots at 0.4 W and an AC signal of 14 V_{pp} at 10 kHz using REP. Reproduced with permission of the Royal Society of Chemistry[78].

surface (Fig. 5a). An illumination intensity of 0.18 W and an AC signal of 14 V_{pp} at 10 kHz trapped 100 nm particles in a single spot on the gold electrode surface (Fig. 5a). Implementing the spatial light modulators, the 100 nm particles were captured in three spots at an increased laser power of 0.4 W (where only 15% of this reached the sample) (Fig. 5b). It must be noted that for nanopatterning REP application, highly smooth surfaces are required to minimize any roughness or imperfection (that is in the order of or greater than the particle size) to deter any localized, non-uniform electrokinetics.

4.1.2 Patterning Bacteria

Most of REP applications discussed so far has focused on the trapping and manipulation of artificial colloids. However, some biological applications were also explored. REP has been shown to trap and manipulate swimming bacteria (*Enterobacter aerogenes*, Fig. 6a–e).[48] In this study, the effects of REP conditions such as the optical radiation and laser induced heating (applied for 4 min) have only shown to indicate insignificant effects on cell viability. It was shown that only high electric fields of 200 k V_{pp} m^{-1} for 5 min caused electroporation in 21% of cell population. REP effectively traps bacteria swimming at average speeds of 23 μm s^{-1} within a parallel ITO electrode chip and fluidic chamber 100 μm in height. At the application of an AC electric field, bacteria (10^7 cells mL^{-1}) suspended in diluted PBS were affected by electro-orientation[46, 51], which results in the polarization and thus an induced dipole along one axis, where the re-orientation is in the vertical direction (direction of electric field) of 98% of the bacteria population. At AC signal of 110 kV_{pp} m^{-1}, 20 kHz, and 20 mW, bacteria were swept by the electrothermal vortex to the stagnation and held there by particle–electrode interactions.

Additionally, REP was used to aggregate and handle various species of bacteria, including

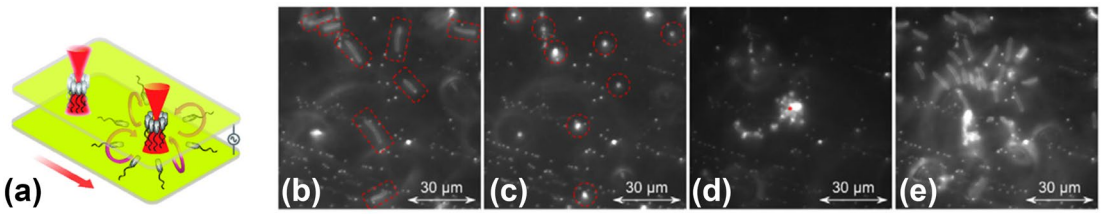

Figure 6: REP used to trap and sort bacteria. **a** *Enterobacter aerogenes* were trapped and translated on an ITO electrode surface at the onset of an electric field of 110 kV_{pp} m^{-1}, 20 kHz, and laser power of 20 mW. Images were acquired for **b** motile *E. aerogenes* before and after **c** the application of electric field. The electric field generated a torque on the bacteria and rotating them vertically, parallel to the direction of the field. **d** Once the laser spot was illuminated on the electrode surface, *E. aerogenes* were accumulated. **e** *Enterobacter aerogenes* lose their vertical orientation and were released once both the AC signal and laser spot were turned off. Reproduced with permission of the Royal Society of Chemistry[48].

Shewanella oneidensis (*S. oneidensis*) *MR-1*, *Saccharomyces cerevisiae* (*S. cerevisiae*), and *Staphylococcus aureus* (*S. aureus*).[38]. For this study, the established experimental setup consisting of the parallel plate ITO chip and Nd: YVO4 laser (1064 nm wavelength) were used. The motile, rod-shaped bacteria *S. oneidensis MR-1* (~1 μm in diameter and 2–3 μm length) were shown to accumulate at an AC signal of 17.8 V_{pp} and 18.7 kHz and a laser of power of 20 mW. The onset of the electric field and laser beam caused over 700 bacteria to align in the vertical direction and be dragged towards the illumination spot by the toroidal microvortex within 0.73 s. Multiple aggregations of bacteria in the same substrate were also formed through two focused laser spots on the substrate. Authors observed that after disabling the AC field and laser spot, bacteria were motile and assumed unharmed by REP effects.

4.1.3 Patterning MWCNTs

REP has the ability to collect and manipulate a single to 100 vertically aligned multi-walled carbon nanotubes (MWCNT) (Fig. 7).[47] The experimental details can be referenced in Mishra et al.[47] publication. Experiments were carried out at 20 mW, with AC electric fields and frequencies between 100–140 kV_{pp} m^{-1} and 10–100 kHz, respectively. Single MWCNTs in deionized water solution (1.3×10^7 CNTs mL^{-1}, 0.37 ± 0.04 mS m^{-1}) were captured and manipulated with a 20 mW laser beam and an AC signal of 140 kV_{pp} m^{-1} and 55 kHz (Fig. 7g–j). The applied electric field produced a dipole moment on the nanotube and generated a torque that flipped the nanotube in the vertical direction, parallel to the electric field. The aggregation of several vertically aligned-MWCNTs was accomplished with a MWCNT solution of 1.6×10^8 CNTs mL^{-1} (0.37 ± 0.04 mS m^{-1}), 20 mW laser beam, and AC field of 140 kV_{pp} m^{-1} at 15 kHz (Fig. 7a–f). Similarly, these nanotubes experienced a torque that aligned them in the direction of the field, while the electrothermal vortex overcome dipole–dipole repulsive forces that increase the separation between the nanotubes.[35] The authors observed that removing the illumination increases the distance between the MWCNTs, while the removal of the electric field causes the MWCNTs to lose their vertical orientation.

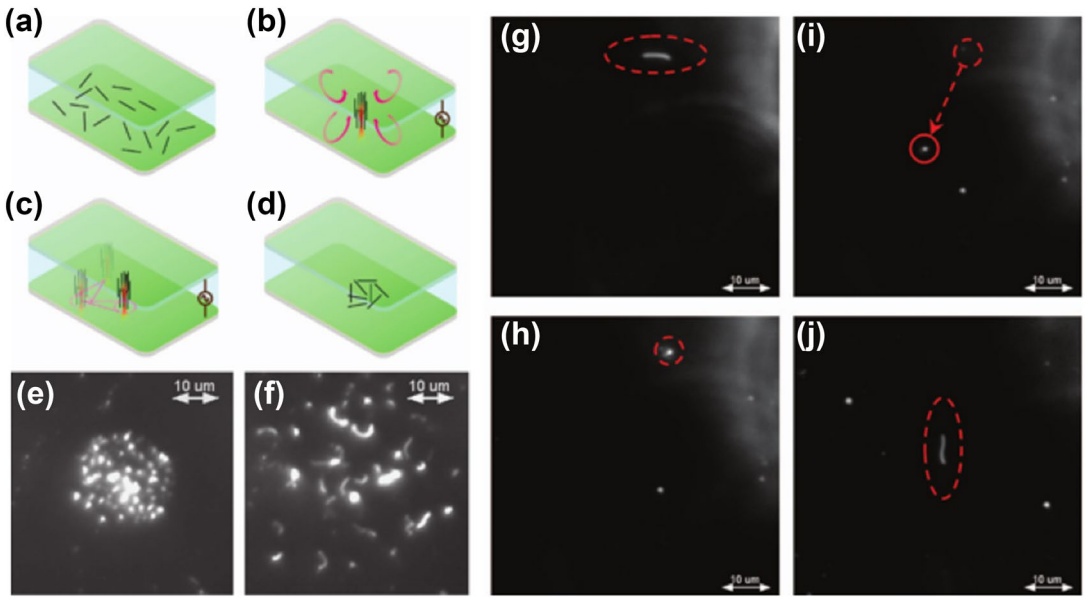

Figure 7: Depictions of **a**–**f** multiple and **g**–**j** single trapped MWCNTs within a REP platform. Diagrams and images of several **a** free MWCNTs and **b**, **e** captured vertically aligned MWCNTs at an AC signal of 140 kV_{pp} m^{-1}, 15 kHz, and laser power of 20 mW. **c** The captured MWCNTs can be translated to a new spot on the surface of the electrode but **d**, **f** lose their vertical orientation and are released from the aggregation once the AC signal and laser spot are deactivated. **g** A single unmanipulated, unaligned and **h** vertically aligned MWCNT after the application of the electric field of 140 kV_{pp} m^{-1} and 55 kHz and laser power of 20 mW. **i** Once trapped, the MWCNT can be translated across the electrode surface. **j** MWCNT was released after the AC signal and laser spot are turned off. Reproduced with permission of Springer Nature[47].

Though REP allows for the dynamic manipulation of MWCNTs, it was also possible to permanent pattern them to the electrode surface by simultaneously applying an AC field of 200 kV_{pp} m^{-1} and DC offset of 12 kV m^{-1}. Experimental observations indicated that the density of the captured MWCNT can be increased by decreasing the AC frequency from 75 to 15 kHz or increasing the solution concentration from 7.8×10^7 to 2.3×10^8 CNTs mL^{-1}.

4.2 Particle Translation

The conventional experimental setup for REP was implemented to translate and rotate particle geometries.[79] The authors show (Figs. 1c, 8a–c) how a particle aggregation of over 600 particles is moved to new spot on the electrode substrate. In this example, the illumination source is deactivated and activated at a short distance away. Initially, the particles scatter and then accumulate in the new spot 40 μm away in under 6 s.

Translation of colloidal aggregation is also possible by combining REP with a scanning near-infrared (NIR) laser system (Fig. 8d–g).[74] The optical experimental components and setup are detailed in Velasco et al.[74] publication. The REP chip in this system consisted of a top electrode plate sputtered with chrome/gold and a bottom ITO coated coverslip. 1.0 μm polystyrene particles were dispersed in aqueous potassium chloride. In this study, particle accumulation was observed at AC signal of 40 kHz at 3.6 V_{rms}, 36 mW laser output power, and scanning periods between 25 ms and 66.7 s. Particle aggregation behavior was affected by the unsteady electrothermal hydrodynamics caused by the scanning laser. Four behavior cases were examined (Fig. 8d–g), the first being a static spot where compact colloidal assemblies are usually observed due to large fluid drag which dominate over dipole–dipole repulsive forces (Fig. 8d).[32, 81] A second case consisted of the translation of the colloidal group (Fig. 5e). This case is observed when the electrothermal fluid velocity exceeds the velocity of the laser. When the speed of the scanning laser is close to or higher than the electrothermal fluid velocity, colloids can be translated with the moving laser but because of dipole–dipole repulsive forces and weaker hydrodynamic drag attractive forces, particles are quickly released (Fig. 8f, g). The study

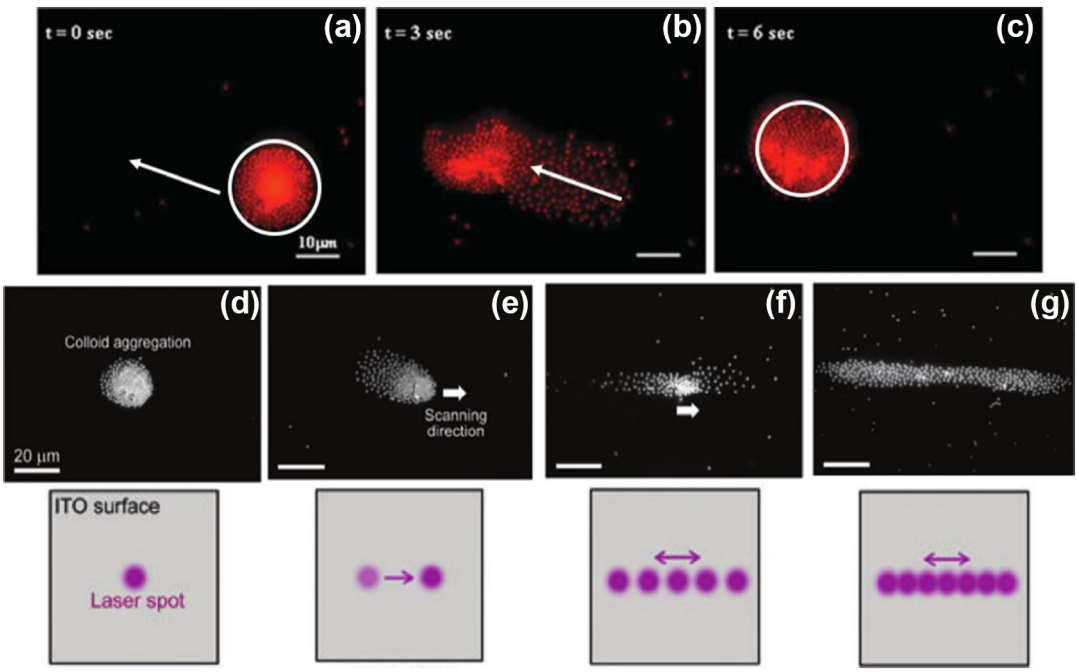

Figure 8: Examples of particle aggregations translated with REP platforms. **a**–**c** Polystyrene particle (690 nm) assembly with over 600 particles were moved when the laser spot was turned off and activated at a spot 40 μm away with an AC signal of 2.0 V_{pp} at 1.6 kHz, an illumination intensity of 20 mW, and the conventional optical setup. Reproduced with permission of the Royal Society of Chemistry.[79] Particles were also translated with a scanning laser system, images show particle assembly behavior during a **d** static the laser spot, as well as, laser scan period of **e** 66.7 s, **f** 6.7 s, and **g** 67 ms. Copyright Wiley–VCH Verlag GmbH & Co. KGaA. Reproduced with permission[74].

showed that to achieve steadier colloidal aggregations, the laser should be programmed to shorter scanning periods. The oscillatory nature of electrothermal fluid dynamics in the scanning REP system could be useful in hydrodynamic drag sorting and micromixing applications.

4.2.1 Translating Bacteria

Similar to the translation of spherical particles, bacteria aggregation was moved to different spot on the electrode surface by repositioning the stage. Bacteria were observed to remain in the vertical orientation and move at the same velocity of the translation of the stage. It was also observed that the alignment of cells is critical for capture, as non-oriented cells have the ability swim and overcome the electrothermal fluid flow.

4.3 Particle Sorting

Particle sorting is also possible through REP (Figs. 1e, f, 9).[33, 81] The frequency dependent behavior of colloidal assemblies in REP makes it possible to sort and characterize particles due to their AC electrokinetic behavior. The critical frequency (Fig. 3b) at which particles are no longer trapped is due to the relaxation polarization of the particle's electric double layer according to Schwarz's fundamental model[63], where particles alike have a critical frequency that is inversely proportional to the particle diameter.

Like previous experimental configurations mentioned above, a parallel ITO electrode chip was used in combination with a near infrared holographic system.[81] 100, 20, and 3 µL of a 2% solids of 2, 1, and 0.5 µm (respectively) carboxylate-modified polystyrene particles (Invitrogen, OR, USA) were suspended in 2.0 mL of potassium chloride solution with a measured conductivity of 2.4 mS m^{-1}. In this study, particles were sorted by size as a result of the frequency-dependent polarization of particles' ionic double layer, where the relaxation frequency is inversely proportional to particle surface area (a^2).[32] All three particles sizes were trapped at AC signal of 38 kHz, 13.4 V_{pp}, and 23 mW (Fig. 9a). Frequency signal was increased to 80 kHz causing the 2.0 µm particles to be discharged leaving the 0.5 and 1 µm particle trapped (Fig. 9b). At a frequency of 106 kHz, the 1 µm particles were released

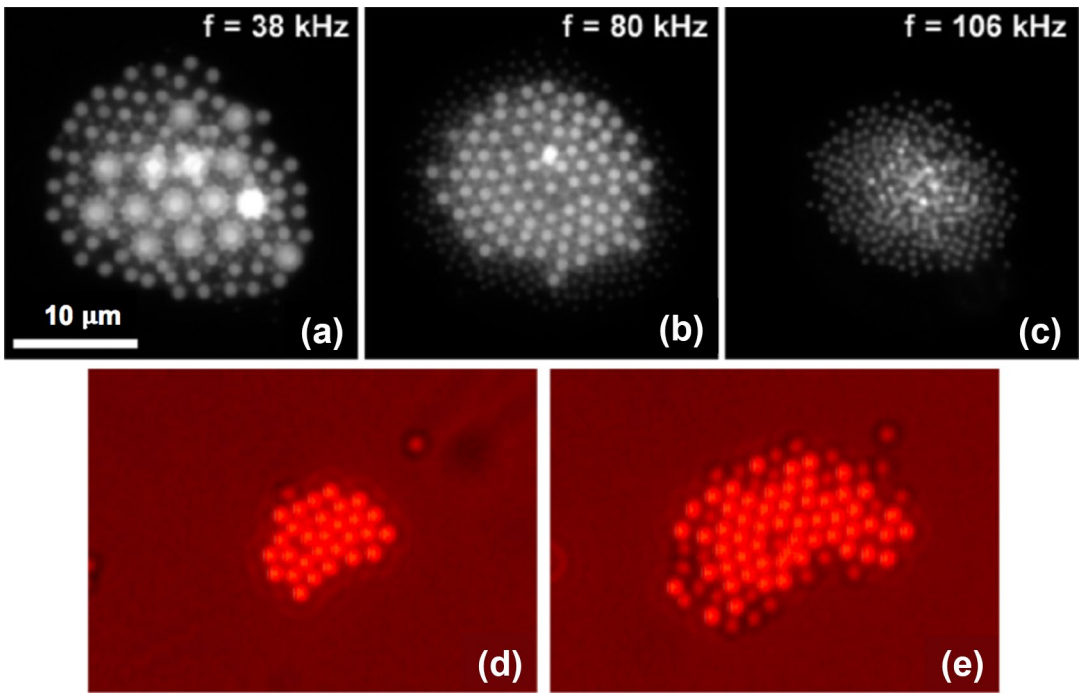

Figure 9: Demonstrations of particle sorting based on **a**–**d** size and **e**–**f** type. **a** All particles (2, 1, and 0.5 µm) were captured 38 kHz, 13.4 V_{pp}, and 23 mW. **b** Increasing frequency to 80 kHz, caused 2 µm to be discharged into the medium, leaving the trapped 1 and 0.5 µm on the electrode surface. **c** At 106 kHz, only 0.5 µm particles remained aggregated. 1 µm polystyrene and silica (non-florescent) were sorted showing REP can characterize particle type. **d** At 150 kHz, 19.8 V_{pp}, and laser power of 23 mW only polystyrene particles were aggregated. **e** At a lower frequency of 90 kHz, both polystyrene and silica particles were captured. Reproduced with permission from IOP publishing[81].

(Fig. 9c). The authors plotted and portrayed a second-order polynomial relationship between the trapping frequency and particle diameter, as well as, AC potential[32, 81], determining that with increasing particle diameter, the critical frequency decreases (Fig. 9c).

Size-based particle sorting was also achieved using the thin film REP chips.[73] In these chips, 1.0 and 2.0 μm particle were trapped at 1.6 V_{DC}, 10 V_{pp}, and 50 kHz. When the AC frequency was increased to 100 kHz, 2.0 μm particles were released.

An alternate way of size-based particle sorting with REP is executed by isolating the larger particle group from a rigid cluster of smaller diameter particles.[78] In this scenario, smaller particles (compared to larger particles) have reduced dipole–dipole repulsive forces and at their minimum inter-particle distance become a rigid particle cluster that resists REP translation. As an example, 0.5 and 1.0 μm polystyrene particles were initially captured at 130 kHz, 25 V_{pp}, and 20 mW. At 50 kHz, the spacing between 0.5 μm particles reached its minimum causing the small diameter particle cluster to become rigid, but leaving the 1.0 μm particle group with ability to move to another location (Fig. S2).

Additionally, the sorting of unlike particles was demonstrated with 1 μm silica and polystyrene particles (Fig. 9d, e).[81] In these experiments, polystyrene particles were captured at 23 mW, 150 kHz, and 19.8 V_{pp}. As the frequency was decreased, silica particles were observed to aggregate at 90–130 kHz. Particle type sorting was observed with a solution conductivity of 2.4 and 4.1 mS m^{-1}. Hence, particle sorting based on particle polarizability, perhaps even surface chemistry (i.e., altered EDL polarizability), is possible.

4.3.1 Sorting Bacteria

In Kwon et al. study, REP was used to separate bacteria taking advantage of the critical frequency of particles emerging from their surface charge density (Fig. 10).[33] For cells with similar surface charges, the critical frequency is assumed as the inverse of particle diameter squared. REP size-based separation was performed on similar zeta-potential *S. cerevisiae* (~5 μm in diameter) and *S. aureus* (~1 μm in diameter) (Fig. 8f–h). Initially, both bacteria were aggregated on the surface at 10.07 V_{pp}, 17.5 kHz, and 20 mW. Increasing frequency to 38.9 kHz caused the larger *S. cerevisiae* to be released with a few of *S. aureus*. Though, authors did not perform viability test, the bacteria was assumed to be unaffected by REP as they remained at the bottom surface and were never visualized floating within the microchannel.

5 Conclusions

Rapid electrokinetic patterning is a technique which combines the advantages of AC electrokinetics and optical energy. The multiphysical nature of this technique offers challenges in developing a comprehensive theoretical model for REP, though significant strides have been made to describe the governing physical mechanisms.

The various capabilities and potentials of REP make it a versatile technique to be applied in a variety of colloidal concentration applications, including creating artificial architectures such as photonic crystals. The frequency-dependent polarization of the particles' or cells' electric double layer can be explored, complementing other electrokinetic techniques like dielectrophoresis that explore interfacial polarization behavior. Rapid aggregation and patterning of colloids is one of the pivotal advantages of REP because it

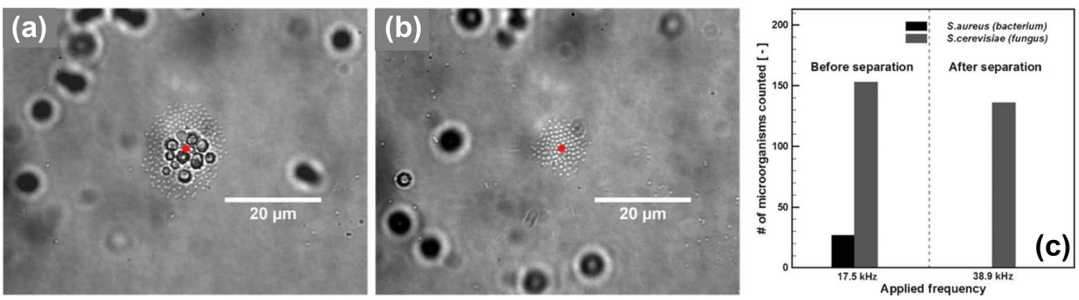

Figure 10: REP used to sort bacteria and shown by Kwon et al.[38], where **a** ***S. cerevisiae*** (~5 μm in diameter) and ***S. aureus*** (~1 μm in diameter) were aggregated on the surface at 10.07 V_{pp}, 17.5 kHz, and 20 mW. **b** Increasing frequency to 38.9 kHz caused the larger ***S. cerevisiae*** to be released with a few of ***S. aureus***. The sorting behavior is plotted in **c** where the relationship between and the number of organisms captured and applied frequency is shown. Reproduced with permission of the Royal Society of Chemistry[38].

enables the development of not only high sensitivity biochemical sensors but also high-performance LOC systems.

Introducing more complex microelectrode structures (ex: interdigitated electrodes) will enable the study of the simultaneous effects of REP and non-uniform electrokinetics like DEP, leading to a new chapter of fundamental and applied research in interface and colloidal science. The REP platform could be modified further with an alternative illumination source. Therefore, the laser used to induce the nonuniform temperature distribution in a conventional REP experiment can be replaced with more low-cost, compact illumination tools like light-emitting diodes, paving the path to development of more portable low-cost microfluidic devices. Inexpensive REP systems with alternative illumination sources and novel electrode materials will extend its range of applications. Constructing a broad illumination REP system creates an inexpensive method of massive parallel particle manipulation and particle assembly that can allow various shape patterning and colloidal aggregations.

REP can be applied to variety of existing lab-on-a-chip techniques such as particle concentration, creation of artificial architectures, microfluidic mixing, and/or pumping. The dynamic control of laser illumination can induce electrothermal flow anywhere on the chip, enabling enhanced, on-demand and reconfigurable microfluidic mixing or pumping. REP's ability to sort, characterize electrokinetic particle behavior, and enhance particle detection will advance many lab-on-a-chip sensing processes because stabilization is essential for accurate diagnostic analysis. The added ability to translate massive particle groups will improve bead-based assays by bringing biologically modified particles into contact with surfaces of interest.

Electronic supplementary material

Below is the link to the electronic supplementary material.Supplementary material 1 (DOCX 3954 kb)

Received: 27 March 2018 Accepted: 10 May 2018
Published online: 31 May 2018

References

1. Adams JD, Kim U, Soh HT (2008) Multitarget magnetic activated cell sorter. Proc Natl Acad Sci 105(47):18165–18170
2. Allen DJ, Accolla RP, Williams SJ (2017) Isomotive dielectrophoresis for parallel analysis of individual particles. Electrophoresis 38(11):1441–1449
3. Arai F, Ng C, Maruyama H, Ichikawa A, El-Shimy H, Fukuda T (2005) On chip single-cell separation and immobilization using optical tweezers and thermosensitive hydrogel. Lab Chip 5(12):1399–1403. https://doi.org/10.1039/b502546j
4. Borlido L, Azevedo A, Roque A, Aires-Barros M (2013) Magnetic separations in biotechnology. Biotechnol Adv 31(8):1374–1385
5. Cetin B, Özer MB, Solmaz ME (2014) Microfluidic bioparticle manipulation for biotechnology. Biochem Eng J 92:63–82
6. Cherukat P, McLaughlin JB (1994) The inertial lift on a rigid sphere in a linear shear flow field near a flat wall. J Fluid Mech 263:1–18
7. Choi S, Song S, Choi C, Park J-K (2009) Microfluidic self-sorting of mammalian cells to achieve cell cycle synchrony by hydrophoresis. Anal Chem 81(5):1964–1968
8. Di Carlo D (2009) Inertial microfluidics. Lab Chip 9(21):3038–3046
9. Di Carlo D, Irimia D, Tompkins RG, Toner M (2007) Continuous inertial focusing, ordering, and separation of particles in microchannels. Proc Natl Acad Sci 104(48):18892–18897
10. Dussaud AD, Khusid B, Acrivos A (2000) Particle segregation in suspensions subject to high-gradient ac electric fields. J Appl Phys 88(9):5463–5473
11. Erickson D, Serey X, Chen Y-F, Mandal S (2011) Nanomanipulation using near field photonics. Lab Chip 11(6):995–1009. https://doi.org/10.1039/c0lc00482k
12. Ermolina I, Morgan H (2005) The electrokinetic properties of latex particles: comparison of electrophoresis and dielectrophoresis. J Colloid Interface Sci 285(1):419–428
13. Evander M, Nilsson J (2012) Acoustofluidics 20: applications in acoustic trapping. Lab Chip 12(22):4667–4676
14. Fagan JA, Sides PJ, Prieve DC (2005) Evidence of multiple electrohydrodynamic forces acting on a colloidal particle near an electrode due to an alternating current electric field. Langmuir 21(5):1784–1794
15. Forbes TP, Forry SP (2012) Microfluidic magnetophoretic separations of immunomagnetically labeled rare mammalian cells. Lab Chip 12(8):1471–1479
16. Friend J, Yeo LY (2011) Microscale acoustofluidics: microfluidics driven via acoustics and ultrasonics. Rev Mod Phys 83(2):647
17. Gaš B (2009) Theory of electrophoresis: fate of one equation. Electrophoresis 30:S1
18. Gong J, Wu N (2017) Electric-field assisted assembly of colloidal particles into ordered nonclose-packed arrays. Langmuir 33(23):5769–5776
19. Green JV, Radisic M, Murthy SK (2009) Deterministic lateral displacement as a means to enrich large cells for tissue engineering. Anal Chem 81(21):9178–9182

20. Green NG, Ramos A, Gonzalez A, Castellanos A, Morgan H (2001) Electrothermally induced fluid flow on microelectrodes. J Electrostat 53(2):71–87
21. Green NG, Ramos A, González A, Castellanos A, Morgan H (2000) Electric field induced fluid flow on microelectrodes: the effect of illumination. J Phys D Appl Phys 33(2):L13
22. Halas NJ, Lal S, Chang W-S, Link S, Nordlander P (2011) Plasmons in strongly coupled metallic nanostructures. Chem Rev 111(6):3913–3961
23. Hayward RC, Saville DA, Aksay IA (2000) Electrophoretic assembly of colloidal crystals with optically tunable micropatterns. Nature 404:56–59
24. Jamshidi A, Neale SL, Yu K, Pauzauskie PJ, Schuck PJ, Valley JK et al (2009) NanoPen: dynamic, low-power, and light-actuated patterning of nanoparticles. Nano letters 9(8):2921–2925
25. Javanmard M, Emaminejad S, Gupta C, Provine J, Davis R, Howe R (2014) Depletion of cells and abundant proteins from biological samples by enhanced dielectrophoresis. Sens Actuators B Chem 193:918–924
26. Jonáš A, Zemanek P (2008) Light at work: the use of optical forces for particle manipulation, sorting, and analysis. Electrophoresis 29(24):4813–4851
27. Jones T (1995) Electromechanics of particles. Cambridge University Press, Cambridge
28. Kang Y, Li D, Kalams SA, Eid JE (2008) DC-Dielectrophoretic separation of biological cells by size. Biomedical microdevices 10(2):243–249
29. Khor JW (2015) Optimizing electrode thickness and material for laser-induced electrothermal flow. Purdue University, West Lafayette
30. Khoshmanesh K, Nahavandi S, Baratchi S, Mitchell A, Kalantar-zadeh K (2011) Dielectrophoretic platforms for bio-microfluidic systems. Biosens Bioelectron 26(5):1800–1814
31. Klepárník K, Boček P (2010) Electrophoresis today and tomorrow: helping biologists' dreams come true. Bioessays 32(3):218–226
32. Kumar A, Chuang H-S, Wereley ST (2010) Dynamic manipulation by light and electric fields: micrometer particles to microliter droplets. Langmuir 26(11):7656–7660
33. Kumar A, Kwon J-S, Williams SJ, Green NG, Yip NK, Wereley ST (2010) Optically modulated electrokinetic manipulation and concentration of colloidal particles near an electrode surface. Langmuir 26(7):5262–5272
34. Kumar A, Kwon J-S, Williams SJ, Wereley ST (2009) A novel optically driven electrokinetic technique for manipulating nanoparticles. In: Optical trapping and optical micromanipulation VI, vol 7400. International Society for Optics and Photonics, p 74000V)
35. Kumar A, Williams SJ, Chuang H-S, Green NG, Wereley ST (2011) Hybrid opto-electric manipulation in microfluidics—opportunities and challenges. Lab Chip 11(13):2135–2148
36. Kumar A, Williams SJ, Wereley ST (2009) Experiments on opto-electrically generated microfluidic vortices. Microfluid Nanofluid 6(5):637
37. Kuzyk A (2011) Dielectrophoresis at the nanoscale. Electrophoresis 32(17):2307–2313
38. Kwon J-S, Ravindranath SP, Kumar A, Irudayaraj J, Wereley ST (2012) Opto-electrokinetic manipulation for high-performance on-chip bioassays. Lab Chip 12(23):4955–4959
39. Kwon J-S, Wereley ST (2013) Towards new methodologies for manipulation of colloidal particles in a miniaturized fluidic device: optoelectrokinetic manipulation technique. J Fluids Eng 135(2):021306
40. Laurell T, Petersson F, Nilsson A (2007) Chip integrated strategies for acoustic separation and manipulation of cells and particles. Chem Soc Rev 36(3):492–506
41. Lenshof A, Magnusson C, Laurell T (2012) Acoustofluidics 8: applications of acoustophoresis in continuous flow microsystems. Lab Chip 12(7):1210–1223
42. Leong T, Johansson L, Juliano P, McArthur SL, Manasseh R (2013) Ultrasonic separation of particulate fluids in small and large scale systems: a review. Ind Eng Chem Res 52(47):16555–16576
43. Lewpiriyawong N, Yang C, Lam YC (2008) Dielectrophoretic manipulation of particles in a modified microfluidic H filter with multi-insulating blocks. Biomicrofluidics 2(3):034105
44. Li M, Li S, Cao W, Li W, Wen W, Alici G (2013) Improved concentration and separation of particles in a 3D dielectrophoretic chip integrating focusing, aligning and trapping. Microfluid Nanofluid 14(3–4):527–539
45. Minden J (2007) Comparative proteomics and difference gel electrophoresis. Biotechniques 43(6):739–745
46. Minoura I, Muto E (2006) Dielectric measurement of individual microtubules using the electroorientation method. Biophys J 90:3739–3748
47. Mishra A, Clayton K, Velasco V, Williams SJ, Wereley ST (2016) Dynamic optoelectric trapping and deposition of multiwalled carbon nanotubes. Microsyst Nanoeng 2:16005
48. Mishra A, Khor JW, Clayton KN, Williams SJ, Pan X, Kinzer-Ursem T et al (2016) Optoelectric patterning: effect of electrode material and thickness on laser-induced AC electrothermal flow. Electrophoresis 37(4):658–665
49. Mizuno A, Nishioka M, Ohno Y, Dascalescu L-D (1995) Liquid microvortex generated around a laser focal point in an intense high-frequency electric field. IEEE Trans Ind Appl 31(3):464–468
50. Morgan H, Hughes MP, Green NG (1999) Separation of submicron bioparticles by dielectrophoresis. Biophys J 77(1):516–525
51. Morgan JT, Wood JA, Shah NM, Hughbanks ML, Russell P, Barakat AI, Murphy CJ (2012) Integration of basal topographic cues and apical shear stress in vascular endothelial cells. Biomaterials 33(16):4126–4135

52. Nadal F, Argoul F, Hanusse P, Pouligny B, Ajdari A (2002) Electrically induced interactions between colloidal particles in the vicinity of a conducting plane. Phys Rev E 65(6):061409
53. Neuman KC, Block SM (2004) Optical trapping. Rev Sci Instrum 75(9):2787–2809
54. Nilsson J, Evander M, Hammarström B, Laurell T (2009) Review of cell and particle trapping in microfluidic systems. Anal Chim Acta 649(2):141–157
55. Pamme N, Manz A (2004) On-chip free-flow magnetophoresis: continuous flow separation of magnetic particles and agglomerates. Anal Chem 76(24):7250–7256
56. Pethig R (2010) Dielectrophoresis: status of the theory, technology, and applications. Biomicrofluidics 4(2):022811
57. Peyman SA, Kwan EY, Margarson O, Iles A, Pamme N (2009) Diamagnetic repulsion—a versatile tool for label-free particle handling in microfluidic devices. J Chromatogr A 1216(52):9055–9062
58. Pohl HA (1951) The motion and precipitation of suspensoids in divergent electric fields. J Appl Phys 22(7):869–871
59. Pohl HA (1958) Some effects of nonuniform fields on dielectrics. J Appl Phys 29(8):1182–1188
60. Ristenpart W, Aksay I, Saville D (2004) Assembly of colloidal aggregates by electrohydrodynamic flow: kinetic experiments and scaling analysis. Phys Rev E 69(2):021405
61. Ristenpart W, Aksay I, Saville D (2007) Electrohydrodynamic flow around a colloidal particle near an electrode with an oscillating potential. J Fluid Mech 575:83–109
62. Rodríguez IA, Tarn MD, Madden LA, Lutz JB, Greenman J et al (2011) Flow focussing of particles and cells based on their intrinsic properties using a simple diamagnetic repulsion setup. Lab Chip 11(7):1240–1248
63. Schwarz G (1962) A theory of the low-frequency dielectric dispersion of colloidal particles in electrolyte solution. J Phys Chem 66:2636–2642
64. Shi J, Huang H, Stratton Z, Huang Y, Huang TJ (2009) Continuous particle separation in a microfluidic channel via standing surface acoustic waves (SSAW). Lab Chip 9(23):3354–3359
65. Song S, Choi S (2013) Design rules for size-based cell sorting and sheathless cell focusing by hydrophoresis. J Chromatogr A 1302:191–196
66. Squires TM, Quake SR (2005) Microfluidics: fluid physics at the nanoliter scale. Rev Mod Phys 77(3):977
67. Suehiro J, Hamada R, Noutomi D, Shutou M, Hara M (2003) Selective detection of viable bacteria using dielectrophoretic impedance measurement method. J Electrostat 57(2):157–168
68. Suwa M, Watarai H (2011) Magnetoanalysis of micro/nanoparticles: a review. Anal Chim Acta 690(2):137–147
69. Tanyeri M, Ranka M, Sittipolkul N, Schroeder CM (2011) A microfluidic-based hydrodynamic trap: design and implementation. Lab Chip 11(10):1786–1794
70. Tay FE, Yu L, Pang AJ, Iliescu C (2007) Electrical and thermal characterization of a dielectrophoretic chip with 3D electrodes for cells manipulation. Electrochim Acta 52(8):2862–2868
71. Thévoz P, Adams JD, Shea H, Bruus H, Soh HT (2010) Acoustophoretic synchronization of mammalian cells in microchannels. Anal Chem 82(7):3094–3098
72. Vahey MD, Voldman J (2008) An equilibrium method for continuous-flow cell sorting using dielectrophoresis. Anal Chem 80(9):3135–3143
73. Velasco V, Williams SJ (2013) Electrokinetic concentration, patterning, and sorting of colloids with thin film heaters. J Colloid Interface Sci 394:598–603
74. Velasco V, Work AH, Williams SJ (2012) Electrokinetic concentration and patterning of colloids with a scanning laser. Electrophoresis 33(13):1931–1937
75. Wang JC, Ku H-Y, Chen T-S, Chuang H-S (2017) Detection of low-abundance biomarker lipocalin 1 for diabetic retinopathy using optoelectrokinetic bead-based immunosensing. Biosens Bioelectron 89:701–709
76. Wang JC, Kumar A, Williams SJ, Green NG, Kim KC, Chuang H-S (2014) An optoelectrokinetic technique for programmable particle manipulation and bead-based biosignal enhancement. Lab Chip 14(20):3958–3967
77. Wang JC, Ku H-Y, Shieh D-B, Chuang H-S (2016) A bead-based fluorescence immunosensing technique enabled by the integration of Förster resonance energy transfer and optoelectrokinetic concentration. Biomicrofluidics 10(1):014113
78. Williams SJ (2009) Optically induced AC electrokinetic manipulation of colloids. Doctoral dissertation in Mechanical Engineering. Purdue University, West Lafayette, Indiana, USA
79. Williams SJ, Kumar A, Wereley ST (2008) Electrokinetic patterning of colloidal particles with optical landscapes. Lab Chip 8(11):1879–1882
80. Williams SJ, Kumar A, Green NG, Wereley ST (2009) A simple, optically induced electrokinetic method to concentrate and pattern nanoparticles. Nanoscale 1(1):133–137
81. Williams SJ, Kumar A, Green NG, Wereley ST (2010) Optically induced electrokinetic concentration and sorting of colloids. J Micromech Microeng 20(1):015022
82. Wood E (1987) Electrophoresis (Analytical chemistry by open learning* series): by Maureen Melvin. pp 130. * ACOL, published by John Wiley & Sons, Chichester, UK.£ 9.95 (pbk) (also available in harback at£ 28) 217–218, ISBN 0-471-91375-8. Biochem Mol Biol Educ 15:4
83. Work AH, Williams SJ (2015) Characterization of 2D colloids assembled by optically-induced electrohydrodynamics. Soft Matter 11(21):4266–4272
84. Wu Z, Hjort K (2009) Microfluidic hydrodynamic cell separation: a review. Micro Nanosyst 1(3):181–192
85. Xuan X, Zhu J, Church C (2010) Particle focusing in microfluidic devices. Microfluid Nanofluid 9(1):1–16

86. Zhang H, Liu K-K (2008) Optical tweezers for single cells. J R Soc Interface 5(24):671–690

87. Zhu J, Xuan X (2009) Dielectrophoretic focusing of particles in a microchannel constriction using DC-biased AC flectric fields. Electrophoresis 30(15):2668–2675

Mohamed Z. Rashed is a graduate student at the University of Louisville in the Department of Electrical & Computer Engineering under the support of a National Science Foundation grant researching dielectrophoresis. Mohamed Rashed received his M.Sc. at Politecnico Di Torino under the support of an EU scholarship. Rashed's ongoing research activities include microfluidics, dielectrophoretic cell characterization, and nano- and micro-fabrication.

Vanessa Velasco has a B.Sc. degree in Chemical Engineering and Biomedical Mathematics from Florida State University. She received her M. Sci. and Ph.D. degree in Mechanical Engineering from the University of Louisville. Her projects have involved the investigation of AC electrokinetic manipulation of particles, the development of microfluidic platforms for in vitro cell analysis, and toxicity studies of carbon nanotubes and graphene on sperm cells.

Stuart J. Williams is an Associate Professor at the University of Louisville in the Department of Mechanical Engineering (microfluidics.louisville.edu). Dr. Williams received his Ph.D. at Purdue University under the support of National Science Foundation Graduate Research Fellowship. Dr. Williams' ongoing research activities include electrokinetic manipulation of colloids for characterization and self-assembly, and colloid self-assembly investigations under microgravity on the International Space Station.